TABLE I. Eigenvalues b for the first few states.

N	b	α
2	−5.08	2.20
3	−16.20	3.99
4	−33.32	5.75
	−5.34	2.26
5	−56.45	7.50
	−20.67	4.52
6	−85.57	9.24
	−42.02	6.46
	−1.63	1.17

Thus for $N=2$ there is one sign change, the one negative eigenvalue. For $N=3$ there is still only one negative eigenvalue. However, for $N=4$ there are two sign changes and so two distinct negative eigenvalues. For higher N, Eq. (26) shows that there are still at least two negative eigenvalues. The remaining analysis is identical to that given in Refs. 6 and 7 for the resonances below the $n=2$ levels Briefly, it utilizes the result of Landau and Lifshitz[12] that an equation which behaves like Eq. (25) with negative $b<\frac{1}{4}$ at large distances has an infinite number of bound states. For the very highly excited bound states, the bulk of the wave function lies in the region where this asymptotic form (25) applies, and its solution can be used to get the dependence of the eigenvalue on the quantum number. The result is

$$\lim_{s\to\infty}\frac{\epsilon_{s+1}{}^{(j)}(N)}{\epsilon_s{}^{(j)}(N)}=e^{2\pi/\alpha_j(N)},\quad \alpha_j(N)=[|b_j(N)|-\tfrac{1}{4}]^{1/2}. \quad (27)$$

Thus, when there is more than one negative eigenvalue of B there will be more than one sequence of infinite eigenvalues of QHQ below the Nth threshold. In Table I we show all the negative eigenvalues and their corresponding values of α_j for the first few N.

Again we should point out that whether these constitute true resonances is in doubt. The value of the lowest eigenvalue of QHQ can be determined by a calculation analogous to that of O'Malley and Geltman with a Q chosen to project out the levels below N, or by a close coupling calculation which includes the levels up to and including N.

ACKNOWLEDGMENT

I am indebted to Dr. R. von Holdt for an illuminating discussion of Sturm's theorem and for obtaining the eigenvalues quoted above.

[12] L. D. Landau and E. M. Lifshitz, *Quantum Mechanics* (Pergamon Press, Ltd., London, 1958), p. 118 ff.

PHYSICAL REVIEW VOLUME 147, NUMBER 1 8 JULY 1966

Resonant Electron Capture in Small-Angle Collisions of Ar^+ on Ar and Ne^+ on Ne†

P. R. JONES, N. W. EDDY, H. P. GILMAN, A. K. JHAVERI, AND G. VAN DYK
Hasbrouck Physics Laboratory, University of Massachusetts, Amherst, Massachusetts
(Received 2 August 1965; revised manuscript received 21 March 1966)

Measurements of the electron capture probability P_0 have been made for single collisions of Ar^+ ions with neutral Ar atoms and Ne^+ ions with neutral Ne atoms, the latter measurements being an extension of work previously reported by this laboratory. The incident ions ranged in energy from 200 eV to 4 keV, the scattered particles being detected at angles ranging from 0.75° to 15° in the laboratory coordinates. A charge analysis of the scattered particles has yielded values of P_0 as a function of the incident ion energy T and scattering angle θ; in both cases P_0 is found to oscillate rapidly as a function of θ, with some dependence upon T also. The periodicity of P_0 as a function of T and θ is consistent with a description of the collision wherein the electronic state of the ion-atom system changes adiabatically and is a superposition of symmetric and antisymmetric energy eigenstates of the diatomic molecular ion. The data are discussed in terms of this description, yielding empirical values of an integral I, defined as the energy difference ΔE between these two eigenstates, integrated over the collision path of relative motion. For the range of collisions studied, I varied from about 6 to 26 eV-Å in the case of Ar^+ on Ar, and from about 5 to 25 eV-Å in the case of Ne^+ on Ne. An approximate functional dependence of ΔE upon internuclear separation R is also obtained, although there is some evidence that ΔE may also depend upon the relative collision speed v in the case of the Ar^+-on-Ar collisions. It is proposed that the ΔE measured for the gentler collisions which produce no excitation of either atomic system is the energy difference between the Π_g and Π_u states of the quasimolecule.

1. INTRODUCTION

THE measurements presented in this paper are a continuation of work previously performed in this laboratory and reported upon in a paper,[1] hereinafter called I. The present measurements of Ne^+ on Ne are an extension of that earlier work to lower incident ion energy T and smaller scattering angle θ. A brief preliminary report of the Ar^+ on Ar measurements presented here was given in another paper.[2]

† This work was supported by a grant from the National Science Foundation.

[1] P. R. Jones, P. Costigan, and G. Van Dyk, Phys. Rev. **129**, 211 (1963).

[2] P. R. Jones, G. Van Dyk, and N. Eddy, in *Proceedings of The Third International Conference on the Physics of Electronic and Atomic Collisions*, edited by M. R. C. McDowell (North-Holland Publishing Company, Amsterdam, 1964), p. 862.

The observation of resonant electron capture in ion-atom collisions was first reported by Ziemba and Everhart[3] in collisions of He^+ on He, and this phenomenon has since been the subject of numerous experimental and theoretical studies, some of which are referred to in I. In addition to the references listed in I there are several recent papers which are particularly relevant to the present study: two theoretical studies by Lichten,[4] an extension of the He^+ on He experiment by Everhart's group,[5,6] and theoretical studies by F. J. Smith[7] and F. T. Smith.[8]

The data of the present paper arise, as in I, from a charge analysis of the scattered particles at various scattering angles θ and for various energies T of an ion beam incident upon a low-pressure target gas. The ratio of the scattered neutral-particle current to the total scattered particle current at any given T and θ is called the neutral fraction P_0, and is interpreted as the electron capture probability for a single ion-atom collision; this paper presents the measured value of P_0 as a function of the two variables T and θ. The measurements were made with better angular resolution and with a more reliable method of determining the incident-ion energy than was the case in paper I.

The interpretation of the data is similar to that presented in I; the collision is described in terms of the impact-parameter method, in which there is a well-defined trajectory of relative motion, and the electronic state is described as changing adiabatically and given by a superposition of symmetric and antisymmetric states of the homonuclear, diatomic molecular ion—the quasimolecule formed during the collision. It is proposed that the observed frequency of oscillation of P_0 is dominated by scattering from the Π_g and Π_u states, ny component of the scattering from the Σ_g and Σ_u states causing a fine structure in P_0 which is not resolved in the present measurements. This description leads to an empirical value of the energy difference ΔE, between the Π_g and Π_u states, integrated over the trajectory of relative motion. An approximate functional dependence of ΔE upon internuclear separation R is also obtained from application of an approximate ion-atom potential energy function, obtained by extrapolating the measured ion-atom potential energy function of Lane and Everhart,[9] and using the classical scattering calculation of Everhart *et al.*[10]

2. APPARATUS

The apparatus used in these measurements is the same as that described and pictured in Fig. 1 of Ref. 1, except for the hole sizes and associated angular resolution. Here, three different sets of hole sizes were used to give what we call coarse resolution, medium resolution, and fine resolution.

The hole sizes for the coarse resolution, medium resolution, and fine resolution, respectively, were as follows: $a=0.042$ in., 0.029 in., 0.018 in. (diam); $b=0.017$ in.$\times 0.030$ in., 0.006 in.$\times 0.030$ in., 0.003 in. $\times 0.030$ in. (rectangular slit); $c=0.029$ in., 0.012 in., 0.0064 in. (diam). Before passing through hole a into the target chamber, the incident ion beam passed through another hole whose diameter was 0.040 in. The maximum angular spread of the main beam, as defined by these two apertures was $\pm\frac{1}{3}$ deg, $\pm\frac{1}{4}$ deg, and $\pm\frac{1}{5}$ deg. The maximum angular spread $\Delta\theta$ of the scattered particles, as determined by apertures b and c, was ± 40 min, ± 18 min, and ± 10 min, respectively, for the coarse, medium, and fine resolutions.

The target-gas pressure was typically 5×10^{-4} torr, a sufficiently low pressure to ensure a preponderance of single scattering over multiple scattering. The pressure outside the target chamber was usually less than 1×10^{-6} torr during operation, falling to a level of about 3×10^{-7} torr when the target-gas supply was shut off.

The scattered particles pass through holes b and c and then traverse the electrostatic analyzer before reaching the detectors. The cylindrical analyzer serves to separate the different charge components of the scattered beam so that each component can be received individually by either of the two detectors, a Faraday cup and a secondary-electron multiplier (SEM). The SEM is a DuMont SP-182 (a ten-stage photomultiplier tube from which the photocathode has been omitted) which has the glass envelope removed to allow the scattered particles to impinge directly upon the first dynode. The output current from each of these detectors is measured by a dc electrometer circuit.

3. METHOD OF MEASUREMENT

A detailed account of our procedure for gathering the data is given in I. The fraction P_0 was determined at each chosen scattering angle θ and incident-ion energy T from the ratio of the neutral-particle current to the total scattered current.

However, in calculating P_0 it was necessary to take account of the fact that the sensitivity of the SEM detector varies with the charge of the incident particle. This was done by method (2) of Ref. 1 wherein apparent oscillations of the total scattered current with changing θ are attributed to oscillations in P_0 together with a lower SEM sensitivity for neutral atoms than for positive ions. Figure 1 shows the relative gain K of the SEM for neutral particles at various kinetic energies, as determined by this method. Here K is defined as the

[3] F. P. Ziemba and E. Everhart, Phys. Rev. Letters **2**, 299 (1959).
[4] W. L. Lichten, Phys. Rev. **131**, 229 (1963); **139**, A27 (1965).
[5] G. J. Lockwood, H. F. Helbig, and E. Everhart, Phys. Rev. **132**, 2078 (1963).
[6] E. Everhart, Phys. Rev. **132**, 2083 (1963).
[7] F. J. Smith, Phys. Letters **10**, 290 (1964): Proc. Phys. Soc. **84**, 889 (1964).
[8] F. T. Smith, Bull. Am. Phys. Soc. **9**, 411 (1964); R. P. Marchi and F. T. Smith, Phys. Rev. **139**, A1025 (1965).
[9] G. H. Lane and E. Everhart, Phys. Rev. **120**, 2064 (1960).
[10] E. Everhart, G. Stone, and R. J. Carbone, Phys. Rev. **99**, 1287 (1955).

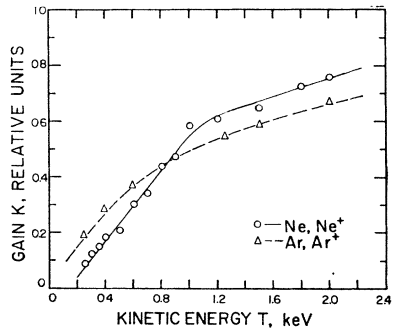

FIG. 1. The relative neutral-particle gain K of the secondary-electron multiplier (SEM) is shown versus the kinetic energy T of the detected particle. K is the ratio of the gain of the SEM for a neutral atom to that for a singly-ionized ion of the same species. The difference between neutral-atom gain and positive-ion gain arises from the first dynode being held at -2 kV, causing the positive ions to strike the first dynode with kinetic energy 2 keV in excess of that shown on the abcissa.

ratio of SEM output currents for equal input particle currents of neutral atoms and singly ionized ions, respectively. Thus the factor K converts the SEM output reading for Ne^+ or Ar^+ ions to a reading which would have been obtained if the SEM sensitivity had been the same for Ne^+ and Ar^+ as for neutral Ne and Ar, respectively.

An improvement in the present measurements over those of I lies in the more reliable determination of the kinetic energy T of the incident ions. The positive ions are produced by rf excitation of a low-pressure gas in an Oak-Ridge-type ion source located inside our high-voltage dome. A voltage V_e is placed between the extraction electrode and the source base, while the dome voltage V_d (with respect to ground) provides further

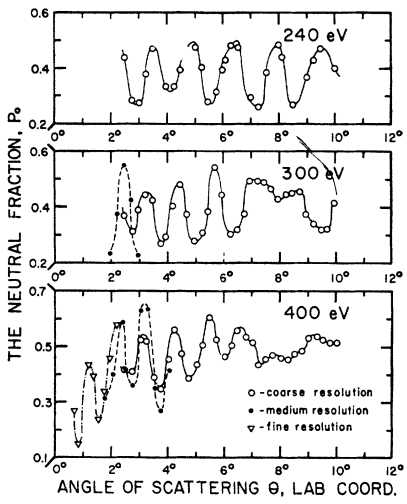

FIG. 2. The neutral fraction P_0 of the scattered incident particles is shown as a function of scattering angle θ at each of several laboratory energies, for single collisions of Ar^+ on Ar. P_0 is regarded as the electron capture probability for the collision. The coarse, medium, and fine resolution data were obtained using successively smaller holes for the main-beam and scattered-beam defining apertures.

acceleration of the ions. In paper I the energy T was taken to be (in electron volts) the sum of V_e and V_d (in volts).

The correct value of the energy T is given by the sum of V_d and V_p, where V_p is the plasma potential relative to the source base. (Here we are ignoring the energy spread due to thermal motion within the plasma.) The fact that V_p may differ from V_e by a rather large amount has been reported in the literature[11] and has also been inferred from our own measurements. The difference $V_e - V_p$ we shall call V_{ep}.

A direct measurement of incident-ion energy T was performed using the cylindrical, electrostatic analyzer pictured in Fig. 1 of Ref. 1. The analyzer was calibrated in the following way: For particles all carrying the same charge, the energy T is proportional to the voltage difference V_a between the analyzer plates. Thus

$$T = CV_a, \tag{1}$$

where C is the analyzer constant (units of eV/V). But T is also given by

$$T = V_d + V_p = V_d + V_e - V_{ep}. \tag{2}$$

Combining (1) and (2) gives

$$V_d + V_e = CV_a + V_{ep}. \tag{3}$$

The procedure was then to vary the dome voltage V_d and observe the corresponding values of analyzer voltage V_a while maintaining all ion-source parameters constant. A plot of $(V_d + V_e)$ versus V_a then gave the analyzer constant C from the slope and the extraction-to-plasma voltage drop V_{ep} from the y intercept.

A significant error in the incident-ion energy T reported in I (called E in that paper) was revealed to us by the measurements just described; for ion-source operating conditions similar to those used in I the voltage drop V_{ep} is about 130 V (± 30 V). Thus, the incident-ion energies reported in I need to be revised downward by 130 eV.

Scattered currents were measured at angles on both sides of the zero-degree setting of the apparatus (i.e., at scattering angles of θ, ϕ and θ, $\phi + \pi$ in spherical coordinates) in order to determine whether the incident-ion beam direction coincided with the zero-degrec direction of the apparatus (as determined by mechanical alignment of the beam-defining apertures). The true beam direction was taken to be that direction about which both the total scattered current and the neutral fraction P_0 showed reflection symmetry. This direction was observed to differ from the zero degree setting of the apparatus by about $\frac{1}{8}$ deg at the lower energies, and much less at the higher energies. (Evidently, the region between the two beam-defining apertures is not completely field free.) The scattering angles reported here are those measured from the symmetry direction.

[11] C. J. Cook, O. Heinz, D. C. Lorents, and J. R. Peterson, Rev. Sci. Instr. 33, 649 (1962).

4. DATA

a. Ar^+ on Ar

Figures 2–4 show the measured neutral fraction, or electron capture probability, P_0 as a function of scattering angle θ at various kinetic energies T of the incident ion in laboratory coordinates. Empirical lines are drawn through the data points. The singly ionized fraction P_1 is simply $1-P_0$ since, in the range of angles and energies shown, there was a negligible amount (<1%) of more highly ionized particles present in the scattered beam. Although there is no way to distinguish between scattered-indicent and recoil-target particles, at these small scattering angles the scattered beam certainly contains a preponderance of the former.[12]

We estimate the accuracy of the data of Figs. 2–4 as follows: the angular location of maxima and minima of P_0, $\pm\frac{1}{8}$ deg; the incident-ion energy T, from $\pm 5\%$ at the lower energies to $\pm 2\%$ at the higher energies. The values of P_0 are also likely to contain more error at the lower energies than at the higher ones since the relative neutral-particle gain K of the SEM, shown in Fig. 1, is such as to cause a much larger correction at the lower energies. Unfortunately, K varies during the lifetime of the SEM, being particularly subject to change after exposure of the dynode surfaces to atmosphere, and cannot be determined with great accuracy by our methods. For example, we attribute the discrepancy between the fine and medium-resolution data at 800 eV (Fig. 3) to uncertainties in the value of K, these data having been taken at rather widely separated times. We place the systematic error in P_0 at $\pm 10\%$ for the higher energies.

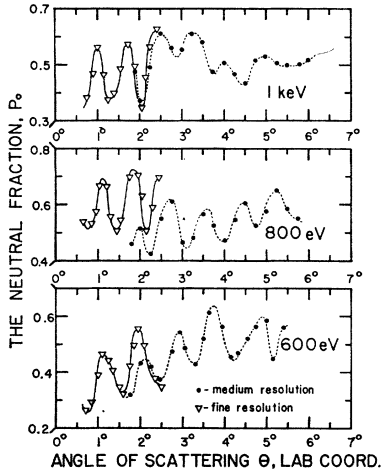

FIG. 3. A continuation of the data of Fig. 2.

Each point in Figs. 2–4 represents the average of two or more points from data runs taken on different days.

[12] Here it is conceptually proper to make the distinction between scattered-incident and target-recoil particles; although the incident and target nuclei are identical, they remain distinguishable throughout the collision by virtue of their nonoverlapping wave functions.

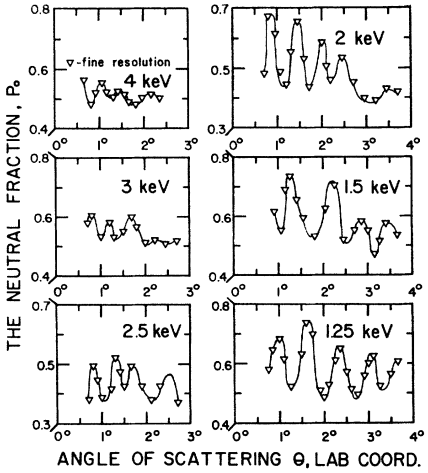

FIG. 4. A continuation of the data of Figs. 2 and 3.

These independent runs showed the P_0 versus θ curves to be, within the experimental error stated above, quite reproducible. The random error in P_0 (i.e., the error aside from that introduced by K, which is believed to be our only source of systematic error) was observed to be less than $\pm 5\%$, when allowing up to $\pm\frac{1}{8}$-deg error in θ.

Use of finer (higher) angular resolution is seen to have generally the expected effect; the maxima in P_0 become larger and the minima become smaller, except as already noted at 800 eV.

The data of Figs. 2–4 are given a partial representation in Fig. 5, which shows the incident-ion energy T

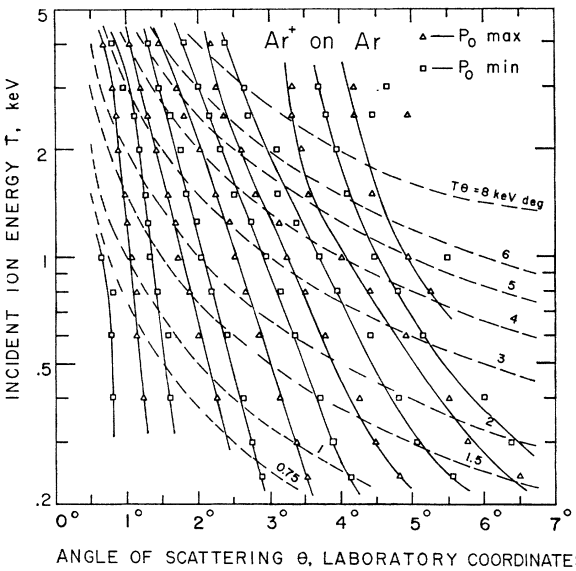

FIG. 5. The data of Figs. 2–4 are used to show here the various laboratory energies and angles for which the neutral fraction P_0 is a maximum or a minimum (i.e., $(\partial P_0/\partial\theta)_T=0$] in single collisions of Ar^+ on Ar. A solid, empirical, line connects the points of each family of maximum P_0 or minimum P_0. The dashed lines of constant $T\theta$ represent curves of constant internuclear distance of closest approach R_0, and are used in further processing of the data.

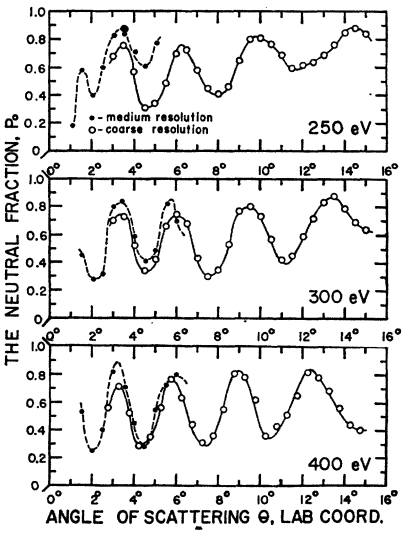

FIG. 6. Data for single collisions of Ne^+ on Ne similar to those shown in Figs. 2–4 for Ar^+ on Ar. These data are also an extension to lower incident-ion energies of the data of Fig. 3, Ref. 1.

and scattering angle θ for each maximum and minimum in P_0. Solid empirical lines connect each family of maxima and minima. More generally P_0 (T,θ) is represented by a surface above the T-θ plane; the solid lines of Fig. 5 locate the ridges and valleys of this surface. The dashed lines of constant $T\theta$ are related to the analysis and interpretation of the data, and will be discussed later.

b. Ne^+ on Ne

Typical data are shown in Figs. 6 and 7 where empirical lines are again drawn through the data points. Again, the singly ionized fraction is 1-P_0. The same estimates of accuracy obtain for these data as for those of Sec. 4(a).

Additional data were gathered at incident-ion energies of 200, 700, and 900 eV, and 1.0, 1.2, 1.5, 1.8, and 2.0 keV, overlapping the data of paper I. All of these data are represented in Fig. 8, which shows also some of the data of I (at energies above 2 keV). Empirical lines again connect families of maxima and minima, locating the ridges and valleys in the $P_0(T,\theta)$ surface. The dashed lines of constant $T\theta$ will be discussed in the next section.

An important difference exists in the interpolation between data points represented by the solid lines of Fig. 5 of paper I and those of Fig. 8 of this paper. In I the oscillations in P_0 occurred in two distinct regions: region 1, where $T\theta$ ($E\theta$ in I) is greater than 20 keV deg and where P_0 has a relatively small mean value and small amplitude of oscillation; region 2, where $T\theta$ is less than about 10 keV deg and where P_0 has a relatively large mean value and large amplitude of oscillation. In the intermediate region, (10 keV deg)$<T\theta<$(20 keV deg), the rapid change in P_0 (best illustrated by the 4-keV data in Fig. 3 of I) generally obscured the location of the local maxima and minima, accounting for the dearth of points in that region of Fig. 5 of I. Considering the location of the points in regions 1 and 2 it seemed probable to us at the time that the local maxima and minima masked by the rapid change in P_0 were actually on the solid lines as shown in Fig. 5 of I.

However, the better angular resolution and more extensive measurements of the present paper have resulted in the location of many more maxima and minima in region 2, and it now seems clear that the interpolation across the intermediate region should be as shown by the dotted and solid lines of Fig. 8. Indeed, the question arises as to the purpose of connecting Regions 1 and 2 in any manner at all; the answer is that while these regions could be treated separately, there appears to be good internal consistency in the data when the two regions are related as shown. This point should become clear in the following section dealing with the interpretation of the data.

5. INTERPRETATION AND DISCUSSION

The interpretation of the data is similar to that given in Ref. 1, wherein the nuclear motion is treated classically in the impact-parameter method (IPM) and the electron motion quantum-mechanically in the adiabatic approximation.

Two of the three criteria for the validity of the IPM are certainly well satisfied by the conditions of the present experiment: (1) the relative wavelength λ is 6×10^{-3} Å or less, while the impact parameter and internuclear distance of closest approach R_0 are between 0.5 and 1.5 Å. (2) The relative angle of scattering is 1.5 deg or larger, while the directional uncertainty $\lambda/2\pi R_0$ is 0.06 deg or less. However, the third condition, that there be a well-defined scattering potential for the collision, requires that the electronic state during the

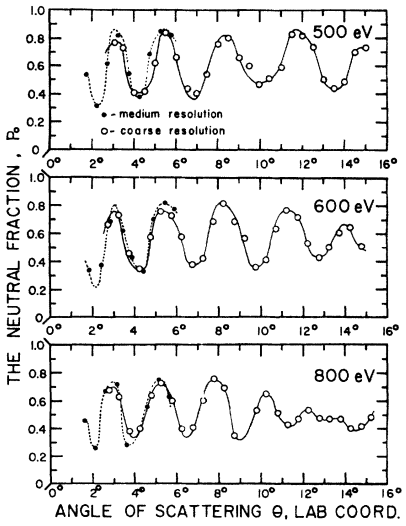

FIG. 7. A continuation of the data of Fig. 6.

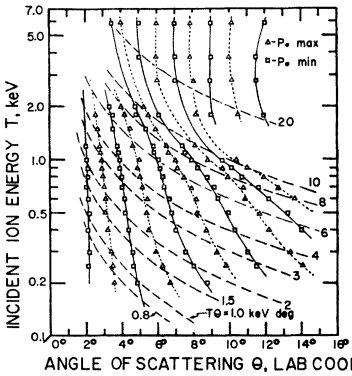

FIG. 8. The data of Figs. 6 and 7 are used to construct for single collisions of Ne^+ on Ne a plot similar to Fig. 5 for Ar^+ on Ar. This plot is an extension of Fig. 5, Ref. 1, to lower energies, and also includes many more points in the energy overlap from 0.8 to 2.0 keV. These added data indicate that the interpolation between 10 and 20 keV deg shown by the solid lines in the earlier work was incorrect; the present drawing of the solid, empirical, lines connecting points of maximum P_0 or minimum P_0 is more consistent with the data.

collision be a definite-energy eigenstate, while in fact the state is a superposition of energy eigenstates. Even so, if the energy difference $\Delta E(R)$ between the eigenstates of the superposition is sufficiently small compared to some empirically determined scattering potential energy $V(R)$ (such as that determined by Lane and Everhart[9]), use of the IPM would appear to be justified. We use the IPM together with $V(R)$ to obtain $\Delta E(R)$ from our data, and then compare $\Delta E(R)$ to $V(R)$.

Since the relative velocity of these collisions is smaller than the classical speed of the outer electrons by a factor of 30 to 60, the electronic state of the ion-atom system should change adiabatically during the collision; a convenient description of the electronic state is given in terms of the adiabatic energy levels of the quasimolecule formed during the collision. The initial electronic state is that of a ground-state neutral atom ($L_1=0$, $S_1=0$) and a ground-state ion ($L_2=1$, $S_2=\frac{1}{2}$) for both the Ar^+ on Ar and Ne^+ on Ne collisions. The projections of the orbital angular momentum on the line joining the nuclei are given by $M_1=0$ for the neutral atom and $M_2=-1, 0, +1$ for the ion. Upon bringing the atomic systems together one has either a Π state, corresponding to $M_2=\pm 1$, or a Σ state, corresponding to $M_2=0$. In addition, there is a doubling of each of these states which can be seen from the twofold degeneracy of each for large internuclear separation R; upon interchange of atomic and ionic states one obtains the same energy. Symmetrizing or antisymmetrizing the wave function of the molecule with respect to this interchange, one obtains the Π_g or Π_u (and Σ_g or Σ_u) states, respectively.[13] The degeneracy of the gerade and ungerade states is removed as R becomes smaller, and it is the interference between such pairs of even and odd states that is primarily responsible for the observed resonance in the electron capture probability P_0 for collisions of positive ions with neutral atoms of the same species.

The principal difference between the Ar^+-Ar and Ne^+-Ne collisions of this paper, and the previously studied He^+-He collisions,[3–6,8] lies in the fact that we have an outer shell of p electrons and not s electrons. Thus we can have not only Σ_g and Σ_u states of the molecule, but Π_g and Π_u as well. However, the description of the collisions is essentially the same whether it be Σ or Π states that are involved; the state is taken to be a superposition of the even and odd states (Σ_g and Σ_u, or Π_g and Π_u) while these states are in turn represented as the sum and difference, respectively, of the two exchange-degenerate, ground-state, ion-atom wave functions.

The expression for the electron-capture probability thus obtained is

$$P_0(T,\theta)=\sin^2(2\hbar)^{-1}\int_{-\infty}^{+\infty}\Delta E dt, \tag{4}$$

where ΔE is (E_u-E_g), the energy difference between the odd and even states respectively. (In Ref. 1 the energies E_r and E_a have the same meaning as the more conventional E_u and E_g of this paper.) The dependence upon T and θ comes through the dependence of ΔE upon the internuclear separation R, which in turn varies with time in a way determined classically by T, θ, and the scattering potential energy $V(R)$. If the angular deflection θ is small, then the relative velocity v remains nearly constant during the collision, and a good approximation to Eq. (4) is

$$P_0(T,\theta)=\sin^2[(2\hbar v)^{-1}\int_{-\infty}^{+\infty}\Delta E ds], \tag{5}$$

where the integration is performed over the path of relative motion. Furthermore, the integral in Eq. (5) will be nearly the same for any two small-angle collisions having the same distance of closest approach R_0 provided ΔE is a rapidly decreasing function of R. Representing this integral as $I(R_0)$, Eq. (5) becomes

$$P_0(v,R_0)=\sin^2[I(R_0)/2\hbar v], \tag{6}$$

where we have achieved a separation of variables in terms of v and R_0.

Equations (5) and (6) give the electron capture probability within the adiabatic, molecular two-state approximation and the IPM for the relative nuclear motion for a collision in *either* the Π_g and Π_u states *or* the Σ_g and Σ_u states; the only difference is that in general the dependence of ΔE upon R will not be the same for the two cases. The scattered particles reaching

[13] The reader is referred to L. D. Landau and E. M. Lifshitz, *Quantum Mechanics*, translated by J. B. Sykes and J. S. Bell (Addison-Wesley Publishing Company, Reading, Massachusetts, 1958); pp. 266–268 are particularly relevant to the present discussion.

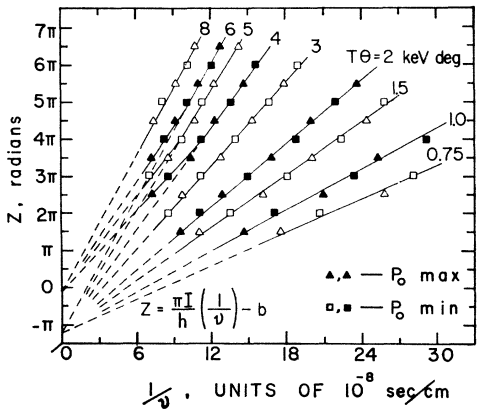

FIG. 9. The data of Fig. 5 are here analyzed in terms of the adiabatic, two-state approximation with a classical trajectory of relative motion for the two nuclei. Each line of constant $T\theta$ represents a family of collisions of constant distance of closest approach R_0. The slope of each line gives the experimental value of I, which is the energy difference ΔE integrated over the collision path. The points for $T\theta=4$, 5, and 6 keV deg appear to lie on two straight-line portions, the break coming in each case at about $v=10^7$ cm/sec, and are considered evidence for the role of other states of the Ar^+-Ar system. The value of the phase constant b cannot be unambiguously determined from our data alone; both values shown are indeterminate to within $n\pi$ (n an integer), although the difference between the two values is fixed as shown at $\sim\pi$.

the detectors should include those resulting from both types of collision, giving a measured value of P_0 which is the weighted sum of two expressions like Eq. (6), one for the Π scattering and one for the Σ scattering:

$$P_0(v,R_0)=\alpha\sin^2[I_\Pi(R_0)/2\hbar v]+\beta\sin^2[I_\Sigma(R_0)/2\hbar v], \quad (6a)$$

where α and β are the fraction of the collisions occurring in the Π and Σ states, respectively. Assuming the projections $M_2=-1, 0, +1$ for the ion to be equally likely, two-thirds of the collisions take place in the Π states, and one-third in the Σ states of the quasimolecule. Thus the periodicity of the observed P_0 as a function of T and θ, or v and R_0, should be that of the Π scattering; the effect of the Σ scattering is then to modulate the observed amplitude of P_0, (the ratio of maximum amplitude to minimum amplitude being 3 to 1) if ΔE_Π and ΔE_Σ are nearly the same, to cause a variation in the observed mean value of the P_0 oscillations if ΔE_Σ is much smaller than ΔE_Π, or to produce a (possibly unobservable) fine structure in the P_0 oscillations if ΔE_Σ is much larger than ΔE_Π. In the case where ΔE_Σ and ΔE_Π have average values for the collision which differ by a factor of about 2 or 3, considerable variety exists in the modifications in P_0 which the Σ scattering can produce, even while the basic frequency of oscillation remains that determined by ΔE_Π.

The data of this paper do not show the detailed structure which Eq. (6a) calls for when $\alpha=\frac{2}{3}$ and $\beta=\frac{1}{3}$. Our interpretation of this fact is that ΔE_Σ is about 2 or 3 times larger than ΔE_Π, and that the second term in Eq. (6a) represents oscillations which are too rapid to be observed with the energy resolution and angular resolution of our measurements.[14]

An empirical modification of Eq. (6) which is consistent with the Ne^+-Ne data of this paper and those of Ref. I, is

$$P_0(v,R_0)=A(v,R_0)+B(v,R_0)\sin^2[I(R_0)/2\hbar v], \quad (7)$$

where both A and B are slowly varying functions of v and R_0. For example, the Ne^+-Ne data in the region $T\theta<$ (8 keV deg) require A and B values of ~0.2 and ~0.6, respectively. These are damped oscillations of P_0 whose possible origins will be discussed in subsection b. below.

A further empirical modification of Eq. (7) is required by the Ar^+-Ar data; the argument Z of the sine must be taken as

$$Z=I(R_0)/2\hbar v-b, \quad (8)$$

where b is a phase constant. Such a phase constant was observed in both the H^+ on H and He^+ on He data of Everhart *et al.*[15,5] and is attributed by Bates and McCarroll[16] to the change in linear momentum of the captured electron.

a. Calculation of $I(R_0)$ and $\Delta E(R)$

The semiempirical expressions of Eqs. (7) and (8) are used, together with the potential energy functions of Lane and Everhart[9] and the classical scattering calculation of Everhart *et al.*,[10] to determine $I(R_0)$ from the data. We use also the functional dependence of R_0 upon the product $T\theta$ as pointed out in Eq. (5) of Ref. 1.

The value of $I(R_0)$ is determined from Eq. (8) by plotting Z versus $1/v$ for each of several families of

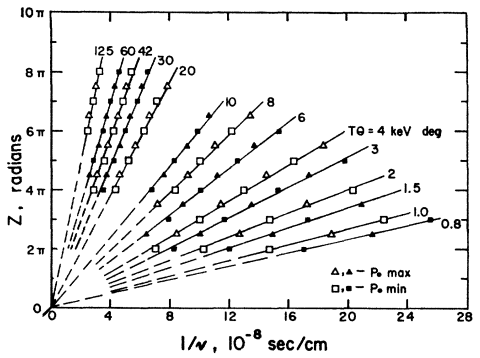

FIG. 10. The Ne^+-Ne data of Fig. 8 are here analyzed in the same way as the Ar^+-Ar data were in Fig. 9. Included also, for $T\theta=20$ keV deg and larger, are the data of Ref. 1. The points lie on straight lines all having the same ordinate intercept, showing the data are consistent with Eq. (7).

[14] We are currently repeating measurements of P_0 in Ne^+ on Ne collisions with better energy and angular resolution and find a reproducible fine structure consistent with Eq. (6a) and a value of $\Delta E_\Sigma\approx3\Delta E_\Pi$. This work is now in progress and will be submitted for publication at a later date.

[15] G. J. Lockwood and E. Everhart, Phys. Rev. **125**, 567 (1962).

[16] D. R. Bates and R. McCarroll, Advan. Phys. **11**, 39 (1962). D. R. Bates and R. McCarroll, Proc. Roy. Soc. (London) **A245**, 175 (1958).

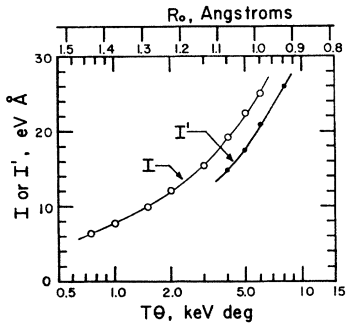

FIG. 11. The slopes of the lines of Fig. 9 are used to determine the experimental value of the integral I as a function of $T\theta$ for the Ar^+-Ar system. Also shown is the relation between $T\theta$ and the internuclear distance of closest approach R_0 determined from the extrapolated Lane-Everhart potential. The two values I and I' correspond to the two families of straight lines of Fig. 9.

collisions of constant R_0, or constant $T\theta$; such families are identified by the dashed lines of Figs. 5 and 8. The intersections of a given dashed line with the various solid (empirical) lines of maximum and minimum P_0 determine the values of $1/v$ and also Z, to within an additive multiple of π, for constant $T\theta$. The plots of Z versus $1/v$ are shown in Figs. 9 and 10; the fact that each family of points of constant $T\theta$ generally lies on a straight line is considered significant evidence for the correctness of the description leading to Eqs. (7) and (8).

Since Z can be determined from our data only to within $\pm n\pi$, where n is an integer, so is the phase constant b indeterminate by an amount $\pm n\pi$. The arbitrary constant was chosen for the Ne^+-Ne data of Fig. 10 so as to make b approximately zero; it was chosen for the Ar^+-Ar data of Fig. 9 so as to make the two values of b shown there either zero or positive.[17] However, $I(T\theta)$ is determined unambiguously from the data, since it depends only upon the slope of Z versus $1/v$.

The Ar^+-Ar data of Fig. 9 are of special interest because they appear to fall into two groups, corresponding to two distinct values of b differing by approximately π. Note also that each of the lines for $T\theta$ values of 4, 5, and 6 keV deg is composed of two straight-line segments, corresponding to two distinct values of I, denoted by I and I' in Fig. 11. The break in the lines[18] occurs in each case at a relative speed $v \cong 1.0 \times 10^7$ cm/sec. The change in b evidently represents a phase shift of π in the odd scattering amplitude produced by rapid rotation of the internuclear axis during the collision.[19] This same rapid rotation of the internuclear axis provides a mechanism for the production of excited electronic states,[20] which can be expected to produce a rather different behavior of P_0 from that predicted by the simple two-state model. Thus the slope I', and the corresponding energy difference $\Delta E'$, should be regarded as phenomenological quantities; perhaps a theory of electron capture in the presence of excitation can identify the states responsible for these oscillations in P_0.

The Ne^+-Ne data of Fig. 10 include also the data from Ref. 1 for the lines 20–125 keV deg; the region from 20 keV deg to about 10 keV deg is characterized by a rapid rise in P_0, the amplitude of the oscillations in P_0 being 10 times as large for $T\theta <$ (10 keV deg) as for $T\theta >$ (20 keV deg).

The slopes of the constant $T\theta$ lines of Figs. 9 and 10 are used to determine values for I, and these are shown in Figs. 11 and 12. Also shown in these figures is the approximate relationship between $T\theta$ and R_0 obtained by extrapolating[21] the measured Ar^+-Ar and Ne^+-Ne potential-energy functions of Lane and Everhart[9] and applying the classical scattering calculation of Everhart *et al.*[10]

The functional dependence of ΔE upon R may be obtained from I versus R_0 by applying a small-angle approximation briefly referred to in Ref. 1 and used also by Everhart in his analysis of He^+-He data[6]: $\Delta E(R)$ is taken to be of the form $C \exp(-R/a)$ and the integration of $\Delta E\, ds$ is performed along a straight-line path which is tangent to the actual trajectory at the

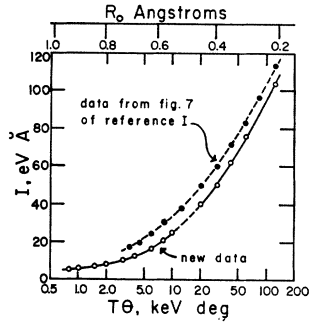

FIG. 12. The integral I is shown versus $T\theta$ and R_0 for the Ne^+-Ne system. The value of I is determined from the slopes of the lines of Fig. 10, and the relation between $T\theta$ and R_0 is obtained from the extrapolated Lane-Everhart potential for Ne^+-Ne. The open points represent new data at the lower energies, and reevaluated old data at the higher energies, and are compared with our earlier measurements of I versus $T\theta$.

[17] We prefer the choice of positive b (negative y intercept) since such a positive value was actually measured for the H^+ on H collision of Ref. 15.

[18] A similar behavior appears in the He^+ on He collision; see Fig. 5 of Ref. 6.

[19] D. R. Bates and D. A. Williams, Proc. Phys. Soc. (London) 83, 425 (1964); F. J. Smith, *ibid.* 84, 889 (1964).

[20] Recent measurements of inelastic energy loss in ion-atom collisions, performed in this laboratory, show that most Ar^+-Ar collisions having $T\theta <$ (3 keV deg) are elastic, while most collisions corresponding to the data group of slopes I' produce excited states. Similar measurements for Ne^+-Ne show that when $T\theta <$ (5 keVdeg) most collisions are elastic, and when $T\theta >$ (15 keV deg) nearly all collisions produce excited states.

[21] The measured potential energy curves of Ref. 9 are shown as nearly straight lines when $RV(R)$ is plotted versus R on a semilog scale (exponentially screened Coulomb potential); we used a straight-line extrapolation of the functions obtained from the 25-keV data. The extent of the extrapolation for Ar^+-Ar was from the 0.3–0.4-Å range out as far as 1.4 Å, and from the 0.1–0.2-Å range out as far as 1.0 Å, for Ne^+-Ne.

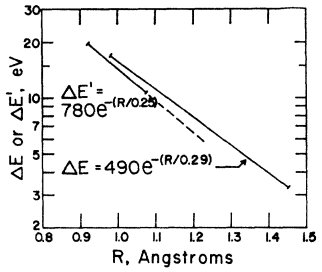

FIG. 13. The measured energy difference ΔE is shown versus the internuclear separation R for the Ar^+-Ar system. ΔE is the empirically determined function which accounts for the data of Fig. 5 via the molecular two-state, adiabatic approximation and a classical internuclear trajectory of relative motion; it is proposed that ΔE is the energy difference between the Π_u and Π_g states. $\Delta E'$ corresponds to the I' of Fig. 11 which represents collisions producing excited states of one or both atomic systems; it should therefore be regarded as a phenomenological function whose identification with particular adiabatic energy levels is not attempted here.

point $R=R_0$. The expression thus obtained is $I(R_0)=2CR_0K_1(R_0/a)$, where K_1 is the first-order modified Bessel function of the second kind. We find that proper selection of the constants C and a gives a good fit between this function and the measured values of $I(R_0)$ shown in Figs. 11 and 12, thus determining $\Delta E(R)$.

Figures 13 and 14 show the experimentally determined functions $\Delta E(R)$. The two functions ΔE and $\Delta E'$ of Fig. 13 correspond to the I and I' of Fig. 11. For the case of Ne^+ on Ne it was necessary to fit the data of Fig. 12 with two choices of C and a, one choice for small $T\theta$ (large R_0) and another choice for large $T\theta$ (small R_0); the result is the two $\Delta E(R)$ functions shown in Fig. 14. The $\Delta E(R)$ function for small R in Fig. 14 should be regarded in the same general way as the $\Delta E'$ function of Fig. 13 for Ar^+ on Ar; because of the extensive excitation[20] produced by these more violent collisions, both I and ΔE should be interpreted as being phenomenological quantities whose precise identification cannot be made on the basis of the simple theory presented here. However, for the larger values of R, particularly where the collisions are mostly elastic, it is proposed that the functions $\Delta E(R)$ of Figs. 13 and 14 represent the energy difference between the Π_g and Π_u states of the $(Ar_2)^+$ and $(Ne_2)^+$ molecular ions, respectively.

The values of $\Delta E(R)$ determined by the above application of the IPM and two-state adiabatic approximation compare with the values of $V(R)$, used in specifying the collision trajectory, as follows: For the Ar^+-Ar system $\Delta E/V$ varies from ~ 0.5 to ~ 0.3 as R varies from 1.4 to 1.0 Å, while for the Ne^+-Ne system $\Delta E/V$ varies from ~ 0.3 to ~ 0.2 as R varies from 1.0 to 0.6 Å. Since ΔE is not very small compared to V, the approximate phenomenological potential energy, the scattering potential energy is really not well defined for the system and the use of the IPM is not entirely justified; the empirical functions $\Delta E(R)$ obtained from the data through application of the IPM must then be regarded as only approximate, not only because of experimental errors in the data and the extrapolation of the Lane and Everhart potential[9] to larger values of R, but because of the indeterminate nature of $V(R)$. We estimate that the probable error in ΔE due to experimental error alone is about $\pm 10\%$.

An appropriate modification of the IPM has been formulated by F. J. Smith,[7] and independently by F. T. Smith,[8] taking into account the effect upon the relative nuclear motion of having a superposition of two scattering potentials, and we shall refer to their results in the following discussion.

b. Damping of the Oscillations

The simple two-state IPM calculation of symmetric charge exchange calls for P_0 to oscillate between unity and zero, in contradiction to previous observations[1–3,5,15] and the data of this paper. Several departures from the simple theory have been shown to yield a reduced amplitude of oscillation.

Transitions to other states are shown by Lichten to produce damped oscillations in P_0; Fig. 7 of Ref. 4 shows the results of a sample calculation for a band of states close to the upper state of a system initially in a superposition of the lowest two molecular states.

Damping within the two-state formulation results from the semiclassical partial-wave analysis of F. J. Smith[7] and F. T. Smith.[8] In this treatment the interference between the gerade and ungerade molecular states applies to the separate, classical trajectories for each of these states as well as to the two electronic states directly; the interference effects at any angle θ are determined by the superposition of final phases ϕ_g and ϕ_u representing E_g and E_u integrated over the classical trajectories for V_g and V_u, respectively. The amplitudes of the gerade and ungerade states are not taken to be equal, as they are in the usual IPM treatment, but are weighted by the square root of the differ-

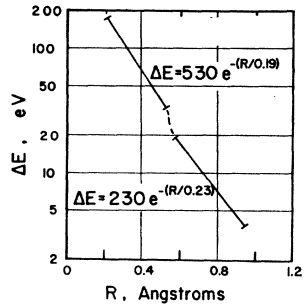

FIG. 14. The empirical function ΔE is shown for the Ne^+-Ne system as it was for the Ar^+-Ar system in Fig. 13. It was necessary to choose different exponential functions, as shown, one for small R and the other for large R, to fit the entire solid curve of Fig. 12. The fact that these two portions of the ΔE versus R curve seem to be discontinuous may be related to the fact that the portion for small R represents collisions producing excitation of one or both atomic systems, while that for large R represents collisions which are mostly elastic. We propose that ΔE for larger R is the energy difference between the Π_u and Π_g states, while ΔE for smaller R be regarded as a phenomenological quantity.

ential scattering cross section $\sigma_g^{1/2}(\theta)$ and $\sigma_u^{1/2}(\theta)$, respectively; it is this unequal weighting which prevents exact cancellation when the two wave functions are out of phase. The expression for $P_{0\max(\min)}$ is obtained at once from Eq. (8) of Ref. 7 as

$$P_{0\max,\min}=(1/2)\pm[\sigma_g(\theta)\sigma_u(\theta)]^{1/2}/[\sigma_g(\theta)+\sigma_u(\theta)]. \quad (9)$$

This latter source of damping would seem particularly pertinent to the small-angle, low-energy Ne^+-Ne data of this paper since these are mostly collisions which leave neither atomic system in an excited state.[20] A rough estimate of the damping predicted by Eq. (9) for Ne^+-Ne collisions is made in the following way: The scattering potential energies $V_g(R)$ and $V_u(R)$, corresponding to the differential scattering cross sections $\sigma_g(\theta)$ and $\sigma_u(\theta)$, respectively, are obtained from the Lane-Everhart potential energy $V(R)$ and our measured $\Delta E(R)$ as

$$V_{g,u}(R)=V(R)\mp(1/2)\Delta E(R)\,. \quad (10)$$

The values of $\sigma_g(\theta)$ and $\sigma_u(\theta)$ are obtained from the classical expressions $2\pi S\ dS=\sigma(\theta)2\pi\sin\theta\ d\theta$, which gives

$$\sigma_{g,u}(\theta)=(S_{g,u}/\sin\theta)(dS/d\theta)_{S=S_{g,u}}, \quad (11)$$

where the impact parameters S_g and S_u correspond to the angle θ for classical scattering from the potential energies $V_g(R)$ and $V_u(R)$ respectively.

It should be noted that Eq. (9) gives unity (or zero) for $\sigma_g(\theta)=\sigma_u(\theta)$, and requires that the ratio $\sigma_u(\theta)/\sigma_g(\theta)$ be quite different from unity in order that there be appreciable damping of P_0. For example, one quickly sees that for $\sigma_u(\theta)=2\,\sigma_g(\theta)$ Eq. (9) gives $P_{0\max}=(1/2)+\sqrt{2}/3=0.97$, and $P_{0\min}=(1/2)-\sqrt{2}/3=0.03$. Our estimate of $\sigma_u(\theta)/\sigma_g(\theta)$ for the Ne^+-Ne data of this paper, obtained through Eqs. (10) and (11), yields a value of 1.2, which in turn yields

$$P_{0\max,\min}=0.998,\quad 0.002. \quad (12)$$

These value of P_0 are in contrast to those of Figs. 6 and 7 where P_0 varies between 0.2 and 0.8. [Similarly, the damping of P_0 predicted by Eq. (9) for H^+-H collisions[7] above 2 keV is very much smaller than that observed.[15]] While there might be a large error in both $V_g(R)$ and $V_u(R)$ due to the extrapolation of the Lane-Everhart potential energy $V(R)$ to larger values of R, it seems very unlikely that this error could be so large as to account for the difference between the damping predicted by Eq. (9) and that observed in the data.

However, much of the damping in the *measured* values of P_0 presented here can be accounted for if two-thirds of the collisions occur in a superposition of Π_g and Π_u states, while the remaining one-third take place in the Σ_g and Σ_u states (i.e., in Eq. (6a) we let $\alpha=\frac{2}{3}$ and $\beta=\frac{1}{3}$), and if the energy separation ΔE_Σ between Σ states is several times that between the Π states. As pointed out earlier, to explain the lack of fine structure in our data, the second term in Eq. (6a) would then represent oscillations in P_0 which would not be resolved by our apparatus.[14] If these high-frequency oscillations were completely unresolved, then this second term would contribute a constant value of $\frac{1}{6}$ to the measured value of P_0, instead of oscillating between 0 and $\frac{1}{3}$. This effect alone would limit the observed oscillations in P_0 to a minimum of 0.17 and a maximum of 0.83. Thus it appears likely that much of the observed damping of P_0 in Ar^+ on Ar and Ne^+ on Ne collisions is jointly an experimental effect and a consequence of scattering from both Π and Σ states.

ACKNOWLEDGMENTS

The authors wish to express their thanks to Professor Edgar Everhart and Professor Arnold Russek of the University of Connecticut for a stimulating discussion of portions of this paper, and to Professor William Lichten of Yale University for a critical reading of a preliminary version of the manuscript.